Magnetoimpedance behavior and its equivalent circuit analysis of Co/Cu/Co/Py pseudo-spin-valve with a nano-oxide layer

Wei-Chih Chien, Yeong-Der Yao, Jiann-Kuo Wu, Chi-Kuen Lo, Ruei-Feng Hung, M. D. Lan, and Pang Lin

Citation: Journal of Applied Physics **105**, 033915 (2009); doi: 10.1063/1.3075841
View online: http://dx.doi.org/10.1063/1.3075841
View Table of Contents: http://scitation.aip.org/content/aip/journal/jap/105/3?ver=pdfcov
Published by the AIP Publishing

Magnetoimpedance behavior and its equivalent circuit analysis of Co/Cu/Co/Py pseudo-spin-valve with a nano-oxide layer

Wei-Chih Chien,[1] Yeong-Der Yao,[2,a)] Jiann-Kuo Wu,[2] Chi-Kuen Lo,[3] Ruei-Feng Hung,[4] M. D. Lan,[4] and Pang Lin[1]
[1]*Department of Materials Science and Engineering, National Chiao Tung University, Hsinchu 310, Taiwan*
[2]*Department of Materials Engineering, Tatung University, Taipei 104, Taiwan*
[3]*Department of Physics, National Taiwan Normal University, Taipei 115, Taiwan*
[4]*Department of Physics, National Chung Hsing University, Taichung 402, Taiwan*

(Received 12 July 2008; accepted 20 December 2008; published online 10 February 2009)

Magnetoimpedance behaviors and thermal effects of a Co/Cu/Co/Py pseudo-spin-valve (PSV) with a nano-oxide layer (NOL) were studied. The PSV can be regarded as a combination of resistances, inductances, and capacitances. In addition, equivalent circuit theory can be used to analyze the ac behavior of this system. The imaginary part of the magnetoimpedance (magnetoreactance) ratio is more than 1700% at the resonance frequency (f_r)=476 kHz at room temperature (R_T). The dc magnetoresistance (MR) ratio decreases as the annealing temperature increases because the NOL is formed at the interface between the spacer and the magnetic layer. The NOL deteriorates the differential spin scattering and reduces the dc MR ratio. Impedance spectroscopy was utilized to analyze the capacitance effect from NOL after annealing. The effective capacitance of the PSV was 21.8 nF at R_T and changed to 11.8 nF after annealing at 200 °C. The useful equivalent capacitor circuit not only is a nondestructive measurement technology but can also explain the experimental results and prove the formation of the NOL. © *2009 American Institute of Physics*.
[DOI: 10.1063/1.3075841]

I. INTRODUCTION

Since the finding of the giant magnetoresistance (GMR) effect in a magnetic multilayer, the pseudo-spin-valve (PSV) has shown great promise for applications in magnetoresistive random access memory, pick-up heads, and magnetic sensors.[1,2] According to a previous report,[3] the growth of PSV films on nano-oxide layers (NOLs) has led to an enhancement in GMR. A corresponding reduction in minimum film resistance by over 10% confirms that this enhancement originates from an increase in the mean free path of spin-polarized electrons due to the resultant of specular reflection on nano-oxide surfaces. Regarding thermal effects of a PSV with NOL, it is well known that formation of another NOL at the interface between the spacer and the magnetic layer degenerates the differential spin scattering. Therefore, the dc MR ratio of the PSV decreases with treatment at higher annealing temperatures.[4] In a nonmetallic system, the impedance (Z) is comprised of resistance (R), inductance (L), and capacitance (C); therefore, equivalent circuit theory can be used to analyze the ac behavior.[5] In our previous work,[6] we utilized the impedance technique to investigate the NOL behavior in PSV. In this study, we extend the impedance technique to report on the frequency response features of the magnetoimpedance (MI) behavior of PSV in more detail and use impedance spectroscopy to conduct nondestructive analysis of a PSV with a NOL after annealing.

Magnetoimpedance, MI=$M|Z|e^{i\theta}$=MR (real part of MI) +iMX, in which $X=X_L-X_C$, of the PSV originates mainly from the inductance and capacitance of the device.[7] It may also contain a small amount of parasitic inductance and capacitance from the wire.[8] For a metallic multilayer such as PSV, X_L usually dominates, with X_C negligible. The hysteresis loop of the PSV and the corresponding behaviors of each component of the impedance, i.e., $|Z|$, θ (phase angle), R, and X, have been carefully examined.

As usual, the MI ratio is defined as $100\% \times (|Z|_{AP} - |Z|_P)/|Z|_P$, where the subscript P (AP) stands for the parallel (antiparallel) magnetization orientation state of the PSV. The magnetophase (MP) ratio, magnetoreactance (MX) ratio, and magnetoresistance (MR) ratio are all defined similarly.

II. EXPERIMENT

A PSV with a NOL of NOL/PSV/substrate was grown by e-gun evaporation at R_T on a thermally oxidized Si (100) wafer with a size of 1×1 cm^2. The NOL was obtained by oxidizing the thin magnetic layers of Co for 10 min naturally. The PSV was Ta 0.6/Co-NOL/Co 3/Cu 5/Co 1/Py 3, where Py denotes $Ni_{80}Fe_{20}$ and all thicknesses shown in brackets are given in nanometers. The base pressure of the growing chamber was lower than 5×10^{-8} Torr, and during the growth, the pressure never exceeds 10^{-7} Torr. The sample was subsequently annealed from R_T to 200 °C for 30 min below the pressure of 1×10^{-2} Torr. The ac behavior was determined by using an HP4194 impedance analyzer with the 16047D fixture. A two-point contact was used in a frequency range from 100 Hz to 40 MHz with a fixed oscillating voltage of ±0.5 V. During the characterization, the ac sensing voltage and external applied field of up to ±100 Oe were applied along the easy axis of the PSV sample, i.e., a longitudinal configuration.

a)Electronic mail: ydyao@phys.sinica.edu.tw.

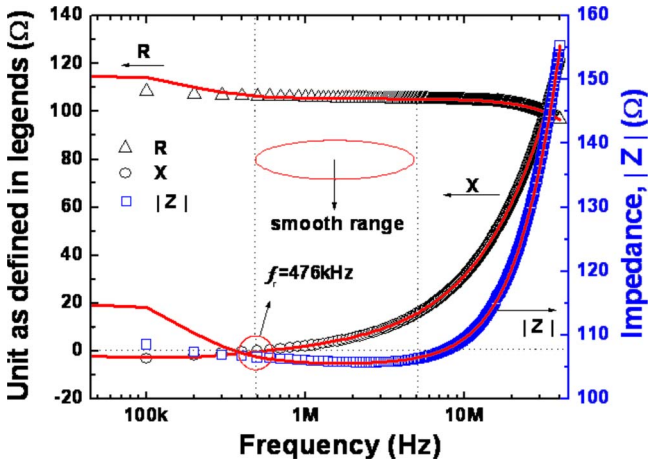

FIG. 1. (Color online) The frequency dependences of $|Z|$, R, and X for the PSV at zero field. The resonance frequency (f_r) is found at 476 kHz, where X vanishes. The experimental data (open symbols) are very close to the theoretical result (solid curves) calculated from the equivalent circuit shown in the inserted panel.

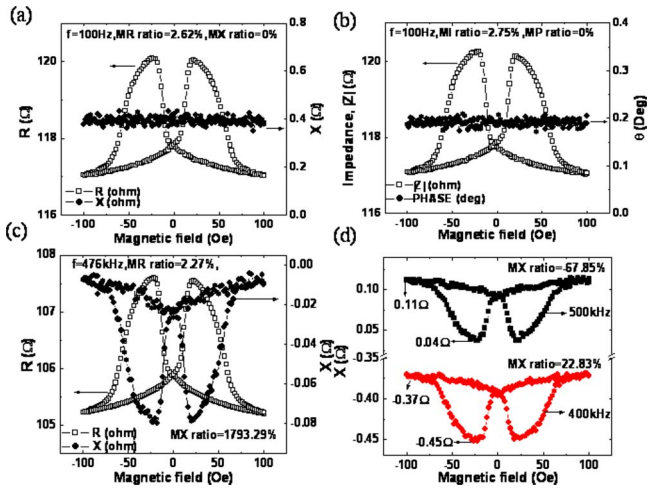

FIG. 2. (Color online) [(a) and (b)] MI at 100 Hz. At this low frequency, the magnetotransport property can be regarded as dc. (c) At resonance frequency f_r (476 kHz), MX shape of loop reverses to MR loop. (d) The value of MX is negative at $f<f_r$, and switches to positive at $f>f_r$.

III. RESULTS AND DISCUSSIONS

Figure 1 shows the frequency dependence of $|Z|$, R, and X for the PSV at zero applied fields. The X curve was negative at low frequency. It turned positive at the frequency $f \geq 476$ kHz, indicative of the resonance frequency (f_r) of the circuit. This is in agreement with the simulated equivalent circuit consisting of an equivalent resistance R_{PSV}(=103.71 Ω), inductance L_{PSV}(=79.85 nH), capacitance C_{PSV}(=20.83 pF), and a parasitic inductance L_P(=627.8 nH), capacitance C_P(=225.04 nF), and resistance R_{P1}(=1.72 Ω), R_{P2}(=12.86 Ω), respectively, as shown in the inset panel in Fig. 1.

The impedance of the equivalent circuit of the PSV is

$$Z = 1/[1/(R_{\mathrm{PSV}} + i2\pi f L_{\mathrm{PSV}}) + (i2\pi f C_{\mathrm{PSV}})] + R_{P1} + i2\pi f L_P + 1/(1/R_{P2} + i2\pi f C_P). \quad (1)$$

The solid line in $|Z|$ shown in Fig. 1 represents the best fit with the experimental data based on Eq. (1). The solid line and the data points fall exactly on top of each other, indicating that the PSV is well represented by the equivalent circuit. Based on this observation, we elaborate on the impedance behavior of PSV under various conditions. The frequency behavior of the PSV, being metallic, is dominated by X_L at high frequency and X_C is significant only at low frequency. Note that X changes from negative to positive as the frequency is swept from 100 Hz to 40 MHz. X vanishes at f_r =476 kHz.

The real part and imaginary parts of the equivalent impedance of the PSV are

$$R_{\mathrm{eff}} = R_{\mathrm{PSV}}/[(1 - 4\pi^2 f^2 C_{\mathrm{PSV}} L_{\mathrm{PSV}})^2 + 4\pi^2 f^2 C_{\mathrm{PSV}}^2 R_{\mathrm{PSV}}^2] + R_{P1} + R_{P2}/(1 + 4\pi^2 f^2 C_P^2 R_{P2}^2),$$

$$X_{\mathrm{eff}} = 2\pi f\{L_P + (L_{\mathrm{PSV}} - 4\pi^2 f^2 C_{\mathrm{PSV}} L_{\mathrm{PSV}}^2 - C_{\mathrm{PSV}} R_{\mathrm{PSV}}^2)/[(1 - 4\pi^2 f^2 C_{\mathrm{PSV}} L_{\mathrm{PSV}})^2 + 4\pi^2 f^2 C_{\mathrm{PSV}}^2 R_{\mathrm{PSV}}^2] - C_P R_{P2}^2/(1 + 4\pi^2 f^2 C_P^2 R_{P2}^2)\}. \quad (2)$$

Note that R decreased very slowly at low frequency and then dropped at a relatively faster pace at higher frequency. This was confirmed by the observation. Furthermore, the $|Z|$ value would have shown a minimum at f_r if the real part of the impedance R had remained constant. In fact, this was not the case. Consequently, the minimum value of $|Z|$ drifted to somewhere between 476 kHz and 5 MHz (smooth range), as indicated in Fig. 1. For the present case, the minimum value of $|Z|$ took place at a frequency near 2.4 MHz, where the slope of the $|Z|$ curve is flat. Beyond this point, the impedance increased rapidly as X_L became dominant. As noted, the capacitance contribution from the equivalent circuit was minimal. Most of the capacitance effect shown in the equivalent circuit had its origin from the parasitic effects of the wire itself.

With the abovementioned Eqs. (1) and (2), the simulation value of the L_{PSV} is 79.85 nH. Let us make a rough order of magnitude estimate of the L value. By definition, $L = BA/I$, where B is the magnetic field, A (7.94×10^{-11} m^2) is the cross section area of the magnetic multilayer through which B passes, and I (4.37 mA) is the current through the sample. The M_s of the PSV measured by VSM is 595.7 emu/cm^3. By simple relation, L is roughly 13.6 nH. This is of the same order of magnitude as observed.

Figures 2(a) and 2(b) show the low frequency response of MI, MP, MR, and MX effects of the PSV at 100 Hz. The behavior of the PSV may be regarded as dc-like at this frequency, and both MX and MP may be treated as frequency independent. On closer inspection, however, the value of the MX at antiparallel state at f_r=476 kHz is clearly nonzero. Interestingly, it shows an inverted negative MR-like loop behavior, as shown in Fig. 2(c). These results are agreement with a previous report.[9] A MX ratio of more than 1700% was observed. This is due to the fact that the imaginary part of Z at parallel state crosses zero at f_r. Figure 2(d) shows that the MX values change from negative (at $f<f_r$) to positive (at $f>f_r$) at 400–500 kHz. The f_r of the PSV is therefore bordering between 400 and 500 kHz in the present sample.

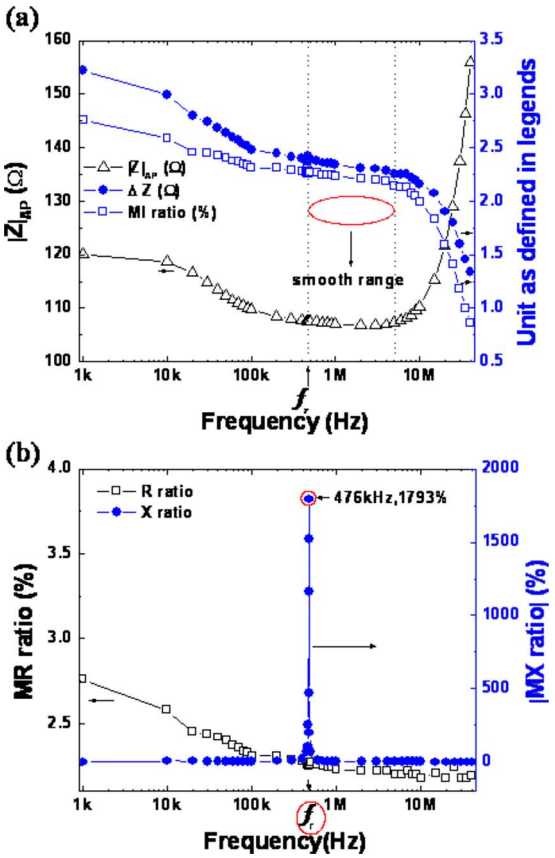

FIG. 3. (Color online) (a) The frequency dependences of $|Z|_{AP}$, ΔZ, and MI ratios. (b) The frequency dependences of MR and |MX ratio|.

Figure 3(a) shows the frequency dependence of $\Delta|Z|$ and $|Z|_{AP}$ and the MI ratio. The behavior of $|Z|_{AP}$ is nearly the same as that of $|Z|$, as shown in Fig. 1. As the frequency increases beyond the smooth range, $|Z|_{AP}$ increases steeply as the X_L increases. It is remarkable that $\Delta|Z|$ decreases slowly but steadily before reaching the smooth range and then decreases sharply upon passing that smooth range. Since the MI ratio was defined as $\Delta|Z|$ divided by $|Z|_{AP}$, it was predictable that the MI ratio would decrease steadily with increasing frequency, as observed.

Based on these observations, it is reasonable to argue that the variation in the impedance $\Delta|Z|$ of the PSV can be simplified as compounded by the parallel and antiparallel states of the moments of the PSV. We have

$$\Delta|Z| = Z_{AP}\text{-}Z_P = 1/[(1/R_{PSV\text{-}AP})^2 + (2\pi f C_{PSV\text{-}AP})^2] - 1/[(1/R_{PSV\text{-}P})^2 + (2\pi f C_{PSV\text{-}P})^2]. \quad (3)$$

Since the R_{PSV} and C_{PSV} depend on the magnetization state, the behavior of the $\Delta|Z|$ is sensitively influenced by the existence (or, effectively, the vacancy density) of the capacitance of the NOL in the PSV and decreases as the frequency increases. The frequency dependences of the MR and the absolute value of the MX ratios are shown in Fig. 3(b). The MR ratio changes only slightly as the frequency changes. In contrast, the |MX ratio| is sharply peaked at the f_r. The value of |MX ratio| is very small at a frequency away from the f_r but shows an astounding peak when X_{AP} is close to zero. A small change in X_{AP} would bring about a great change in the |MX ratio| (~1793% in the present sample).

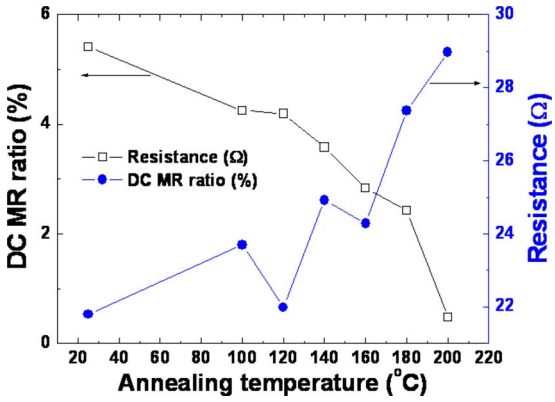

FIG. 4. (Color online) The dc MR ratio and resistance (r) of the PSV are functions of the annealing temperature.

The dc MR ratio of the PSV decreased as the annealing temperature increased, which occurred because NOL formed in the interface between the spacer and the magnetic layer. For this reason, we used the impedance technique to analyze the capacitance effect, which is caused by oxidation. Figure 4 shows that the resistance of the PSV increased from 21.80 to 28.98 Ω and the dc MR ratio of the PSV decreased from 5.41% to 0.48% as the annealing temperature increased from R_T to 200 °C, which indicates that oxidation occurred in the PSV. Therefore, the effective capacitance was measured by imaginary part of impedance [Im(Z)] curves, as shown in Fig. 5. Im(Z) reached a minimum at roll-off frequency (f_{roll}). The plot of f_{roll} as a function of annealing temperature is shown in Fig. 6; f_{roll} increased linearly from 345 to 465 kHz at annealing temperatures from R_T to 200 °C. It is quite interesting to analyze the effective capacitance effects with changes in annealing temperature. According to the effective capacitance calculation, f_{roll} can be shown as

$$f_{roll} = 1/(2\pi R_{eff} C_{eff}). \quad (4)$$

The effective capacitance is in reverse proportion to the f_{roll} and estimated values, and it varies from 21.8 to 11.8 nF as annealing temperatures increases from R_T to 200 °C. One possible explanation is that the effective capacitance decreases as annealing temperature increases by hysteresis loops, as shown in Fig. 7. The coercivity (H_c) of Co is 20

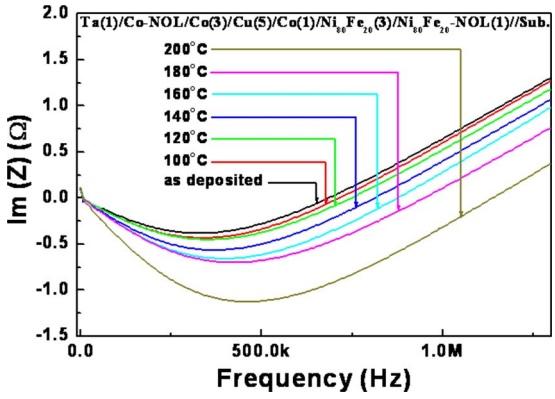

FIG. 5. (Color online) Imaginary part of impedance curves for PSV with different annealing temperatures ranging from R_T to 200 °C.

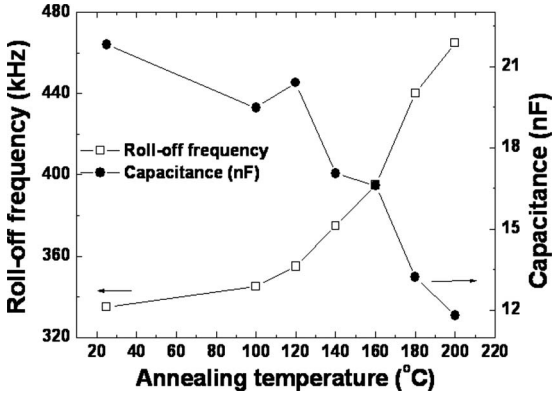

FIG. 6. The roll-off frequency and effective capacitance of the PSV are functions of the annealing temperature.

Oe, and the H_c of Co–Py coupled is 12 Oe in the PSV, which was deposited at R_T. When the annealing temperature was increased to 140 °C, the H_c of Co was apparently incoherent in the PSV, indicating that the oxidation effect occurred in the Co layer. The oxidative thickness is in proportion to f_{roll} and in reverse proportion to C_{eff}.[6] The result of f_{roll}, which increased as annealing temperature increased to 140 °C, indicated that the oxidative thickness of Co layer was increasing. This increase in thickness caused the resistance to increase and the dc MR ratio to decrease slightly. Above the annealing temperature of 140 °C, it is difficult to distinguish the H_c of Co or that of Co–Py, implying that the oxidation effect occurs in the Co/Cu or Co–Py/Cu interfaces. They could be regarded to two capacitors in series, thus causing a decrease in effective capacitance, as shown in the inset panel in Fig. 7. Therefore, the f_{roll} increases and effective capacitance decreases as the annealing temperature increases, indicating that the increase in annealing temperature causes the oxidative thickness to increase and oxidize more than one layer.

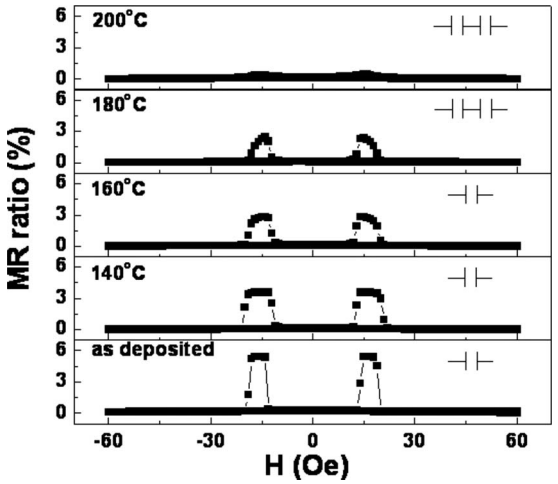

FIG. 7. The hysteresis loops of the PSV with annealing temperatures at R_T, 140, 160, 180, and 200 °C, respectively. The inset panels show the equivalent capacitor modes.

IV. CONCLUSION

In conclusion, the ac behavior in the PSV led to interesting MR and MX loops, with the MR loop a reversal of the MX loop. The MI effect of PSV has been investigated at R_T. It is found that the PSV can be regarded as a combination of resistances $(R_{\text{PSV}}, R_{P1}, R_{P2})$, inductances (L_{PSV}, L_P), and capacitances (C_{PSV}, C_P), and equivalent circuit theory can be used to analyze the ac behavior of this system. It is quite interesting that the $|\text{MX}|$ ratio is more than 1700% at f_r =476 kHz. This suggests strongly that PSV is potentially a very sensitive frequency sensor. The MI behavior in the Co/Cu/Co/NiFe PSV with a NOL after annealing treatment has also been studied. Its roll-off frequency increases from 345 to 465 kHz, and the effective capacitance decreases from 21.8 to 11.8 nF as the annealing temperature increases from R_T to 200 °C. We can utilize the equivalent capacitor circuit to explain the NOL behavior with annealing temperature. This study shows that impedance analysis is a useful technique, and its nondestructive measurement should be more widely appreciated.

ACKNOWLEDGMENTS

This work was supported in part by the National Science Council of Taiwan under Grant No. NSC 95-2112-M-036-002-MY3 and in part by the Nano-program at Academia Sinica.

[1]N. Baibich, J. M. Broto, A. Fert, F. Nguyen Van Dau, F. Petroff, P. Creuzet, A. Friederich, and J. Chazelas, Phys. Rev. Lett. **61**, 2472 (1988).
[2]B. Dieny, V. Speriosu, B. Gurney, S. Parkin, D. Wilhoit, K. Roche, S. Metin, D. Peterson, and S. Nadimi, J. Magn. Magn. Mater. **93**, 101 (1991).
[3]M. Mao, C. Cerjan, and J. Kools, J. Appl. Phys. **91**, 8560 (2002).
[4]C.-H. Lai, C. J. Chen, and T. S. Chin, J. Appl. Phys. **89**, 6928 (2001).
[5]W. C. Chien, C. K. Lo, L. C. Hsieh, Y. D. Yao, X. F. Han, Z. M. Zeng, T. Y. Peng, and P. Lin, Appl. Phys. Lett. **89**, 202515 (2006).
[6]W. C. Chien, T. Y. Peng, L. C. Hsieh, C. K. Lo, and Y. D. Yao, IEEE Trans. Magn. **42**, 2624 (2006).
[7]M. F. Gillies, A. E. T. Kuiper, R. Coehoorn, and J. J. T. M. Donkers, J. Appl. Phys. **88**, 429 (2000).
[8]K. Okada and T. Sekino, *Impedance Measurement Handbook* (Agilent Technologies Co., Santa Clara, CA, 2003), pp. 2–18.
[9]H. Kaiju, S. Fujita, T. Morozumi, and K. Shiiki, J. Appl. Phys. **91**, 7430 (2002).